X3.19 EGU2018-9753

LA-UR-18-22872

Overall energy budget of earthquake rupture with dynamically generated off-fault crack network

Kurama Okubo*[1,2], Harsha S. Bhat[2], Zhou Lei[3], Earl E. Knight[3], Esteban Rougier[3] and Yann Klinger[1]

[1] Institut de Physique du Globe de Paris, Tectonique et mécanique de la lithosphère [2] École Normale Supérieure, Laboratoire de Géologie, Paris, France [3] Los Alamos National Laboratory, NM, United States *okubo@ipgp.fr

Introduction: Complex fault system from small to large length scale

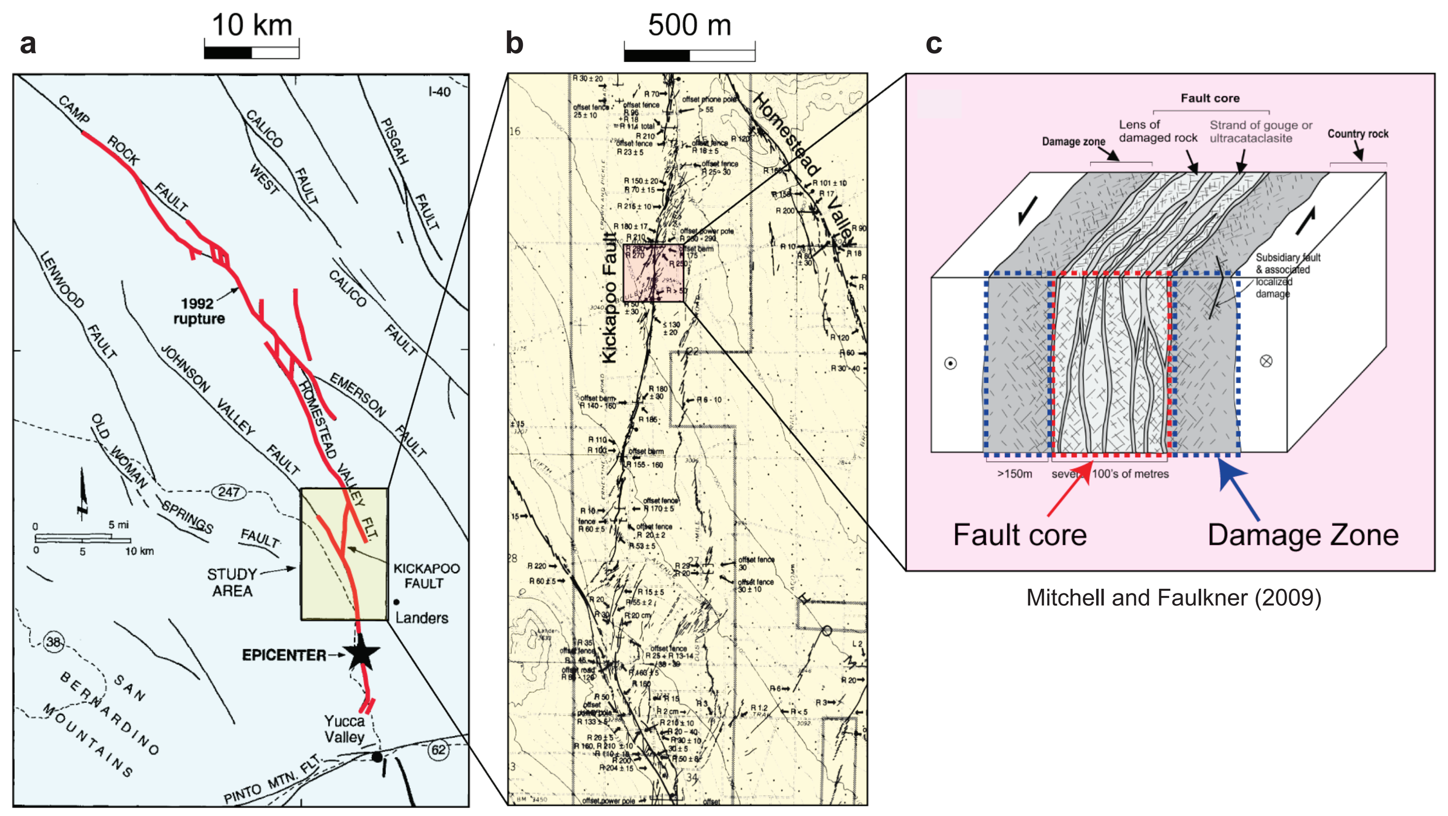

Sowers et al. (1994) Courtesy of Harsha S. Bhat — Sowers et al. (1994) — Mitchell and Faulkner (2009)

The natural fault system can be decomposed into **hierarchical structure of different length scales**. The natural fault network is usually composed of many faults as shown in Fig. (a). When we focus more, we can find smaller scale crack network around main faults (Fig. b), which is the so called off-fault damage. Further down in length scale, the localized shear band, called fault core (Fig. c), can be observed and is surrounded by micro-scale fractures. Our goal is to understand **the role of off-fault fracture network** induced by dynamic earthquake rupture propagating along fault networks **on the earthquake rupture dynamics and the associated radiation**.

Methodology: Continuum-discontinuum analysis using FDEM

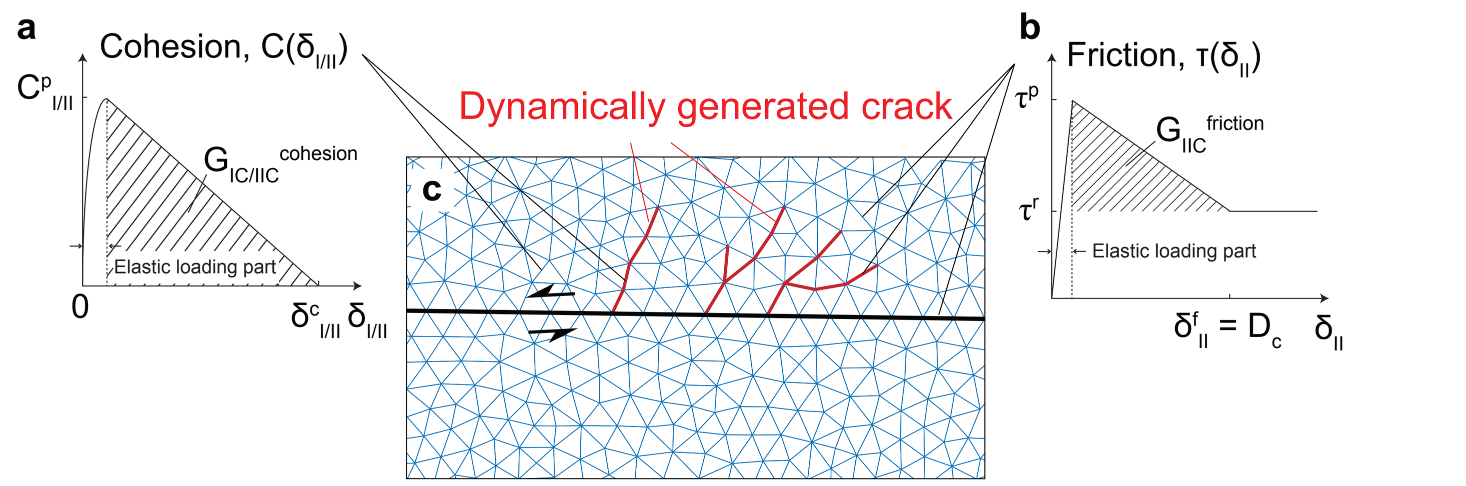

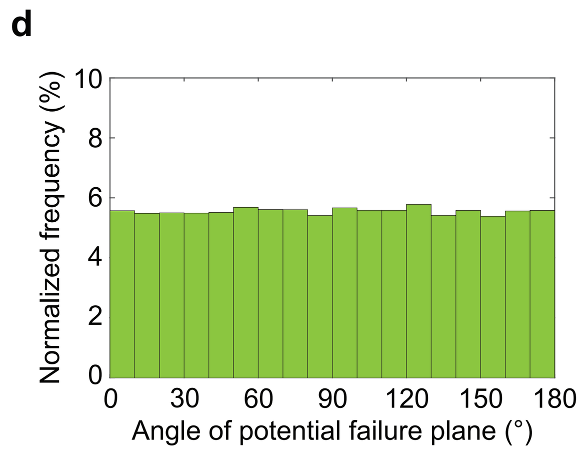

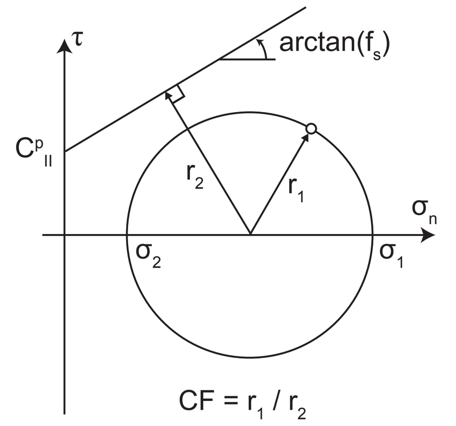

We use a continuum-discontinuum based scheme, **the combined finite-discrete element method (FDEM)**, to achieve both high-numerical accuracy of rupture propagation, seismic wave radiation and to model the activation of new cracks, in both tension and shear, in the off-fault medium.

(a) Linear softening cohesion curve. $\delta_{I/II}$ is the amount of slip in tensile (mode I) and shear (mode II). $C^p_{I/II}$ is the peak strength in tensile and shear cohesion. $\delta^c_{I/II}$ is the critical normal/tangential displacement for softening of tensile/shear cohesion. $G_{IC/IIC}^{cohesion}$ is the dissipated energy by breaking cohesion. (b) Linear slip-weakening curve. δ^f_{II} is the characteristic slip distance which is identical with the D_c in conventional slip-weakening law. τ_p and τ_r are the peak and residual strength in friction, derived as $\tau_p = f_s\sigma_n$ and $\tau_r = f_d\sigma_n$, where σ_n is the compressive normal stress on the boundary of elements. $G_{IIC}^{friction}$ is the fracture energy dissipated by the frictional process. (c) Zoomed window around faults. Black solid line shows the prescribed fault and blue lines show the discrete finite elements. Red lines show the newly generated cracks on which the cohesion starts to decrease. (b) Histogram of the angle of potential failure plane.

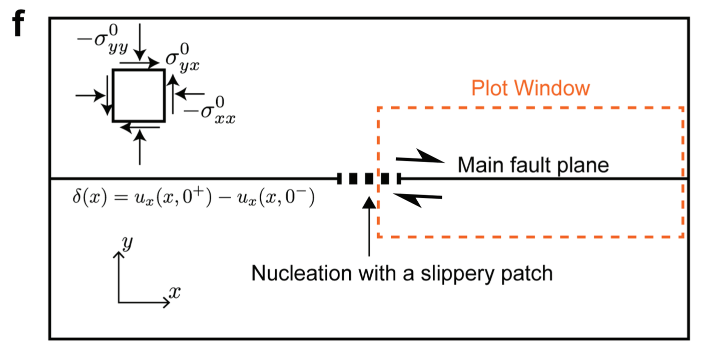

(e) Schematic of closeness to failure CF defined as r_1/r_2, which is used for the parametrization of failure criteria such as peak cohesion. (f) Model description of single planar fault. We model strike-slip rupture which is artificially nucleated at the middle of the fault by setting less peak strength. Since the rupture propagates bilaterally, the dynamic rupture and coseismic off-fault damage pattern are symmetric with respect to x=0. We thus plot only the right side of the medium. The top half is the compressive side and bottom half is the extensional side in the plot window.

Result: Dynamic earthquake rupture with coseismic off-fault crack network

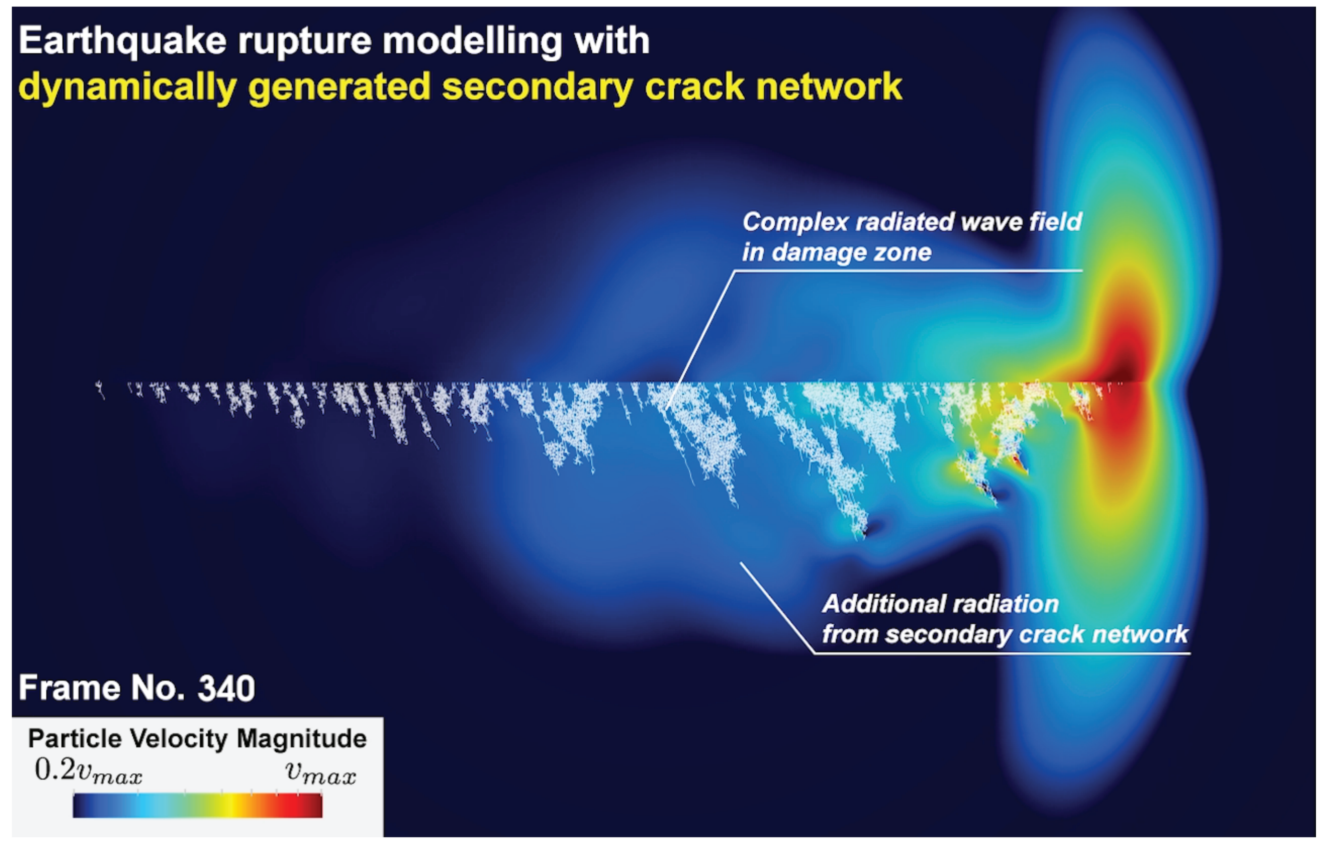

Snapshot of dynamic earthquake rupture with coseismic off-fault crack network. Color contour shows the particle velocity magnitude. White lines show the dynamically activated off-fault crack network. Rupture is nucleated to the left of the plot window. Rupture velocity increases as the rupture propagates, leading to the wider width of the damage zone. The pre-stress condition is chosen to nucleate a sub-Rayleigh rupture. We clearly see the perturbed radiation field due to the off-fault damage, which contributes to the high-frequency part of the acceleration in spectrum.

High-frequency radiation from off-fault secondary cracks

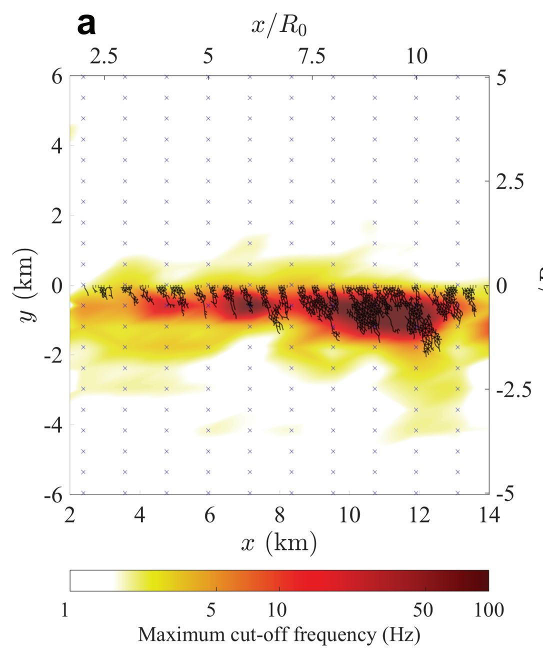

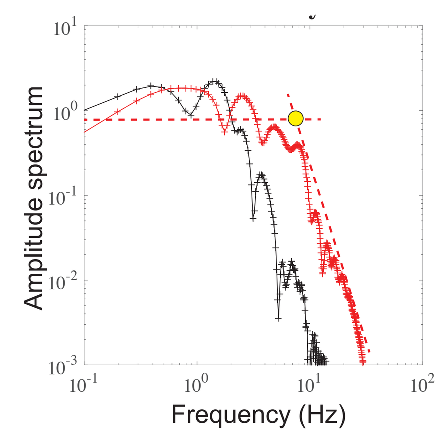

(a) Spatial distribution of maximum cut-off frequency in acceleration amplitude spectrum. We put the sensors (seismic stations) everywhere in the medium and obtained the acceleration amplitude spectrum. Then we estimate the maximum cut-off frequency at each position. (b) An example of the spectrum. We run two calculations; one is with coseismic off-fault damage (shown in red) and the another is with purely elastic model, which does not allow for off-fault cracking (shown in black).

It clearly demonstrates **the enhanced high-frequency radiation especially in the damage zone** and its rapid attenuation with distance.

Distribution of the orientation of off-fault cracks in depth

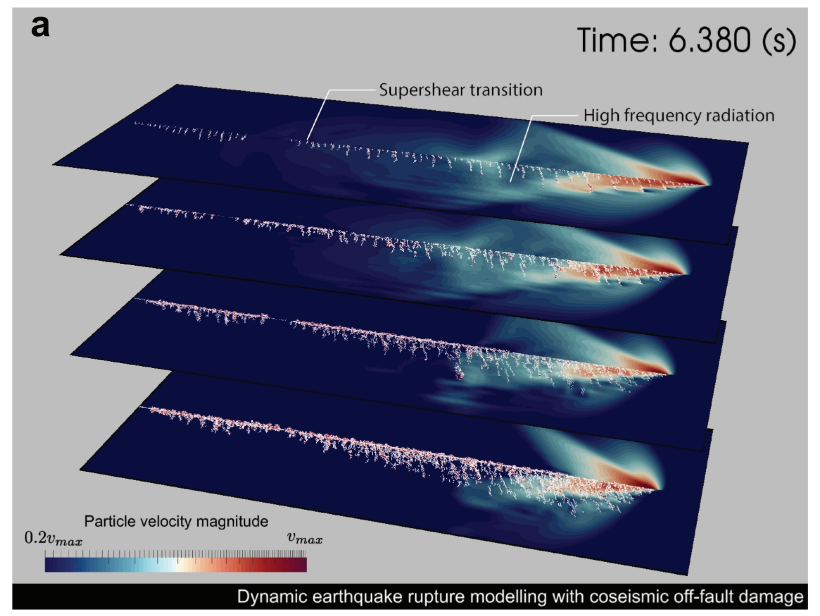

We conducted case study in depth by increasing both normal and shear traction on the fault that follow a lithostatic gradient..

(a) Snapshot of case study. We have four 2D slices in depth and we simulate each depth case separately. It is worth noting that the pre-stress condition in this section is preferable for transition to super-shear rupture and the process/cohesive zone size R_0 is kept constant for the sake of demonstration. We show the case study in depth with constant G_{IIC} in the section of damage zone width, which is regarded as a more realistic assumption. (b) Trace of secondary off-fault cracks and histogram of the crack orientation with respect to the fault. It shows a broader distribution of crack angle in deeper (high compression) case, which implies that more intricate crack network can be formed in deeper parts of the fault.

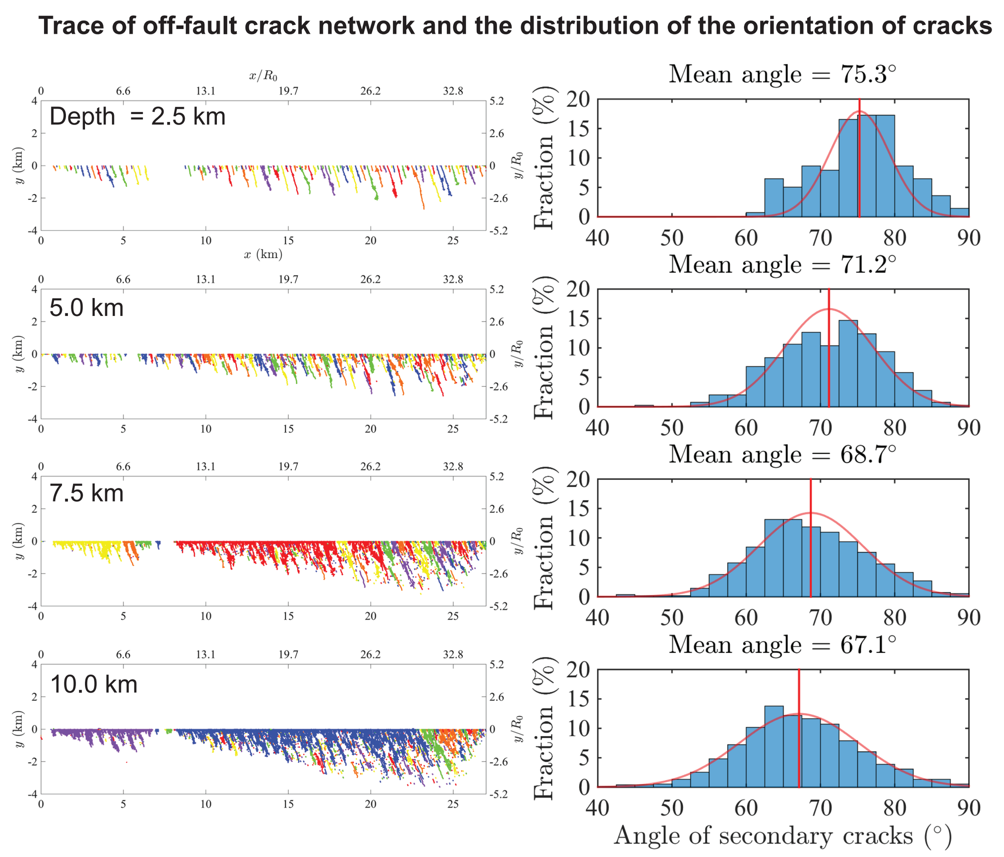

Overall energy budget of dynamic rupture with coseismic off-fault crack network

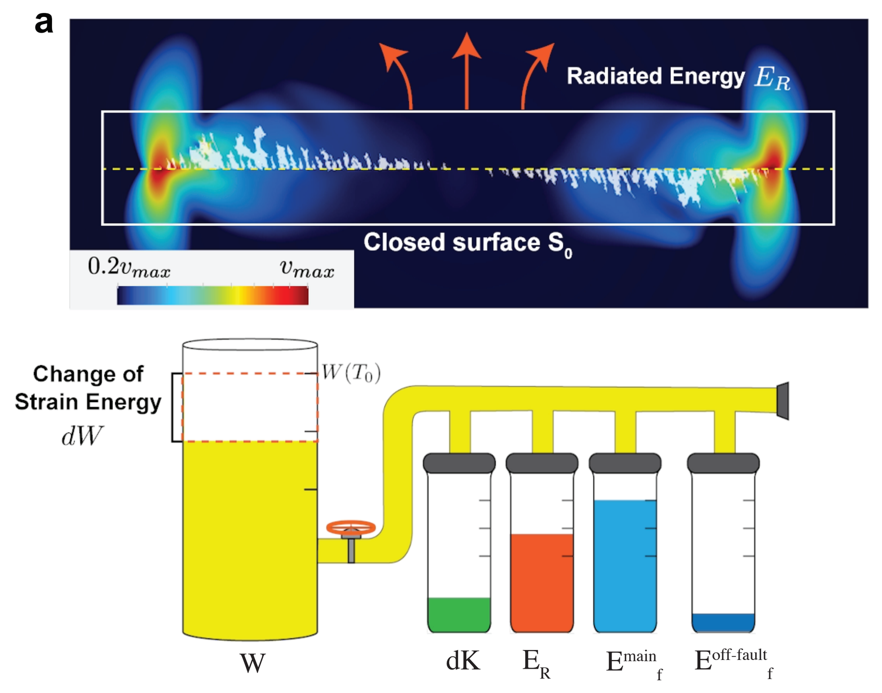

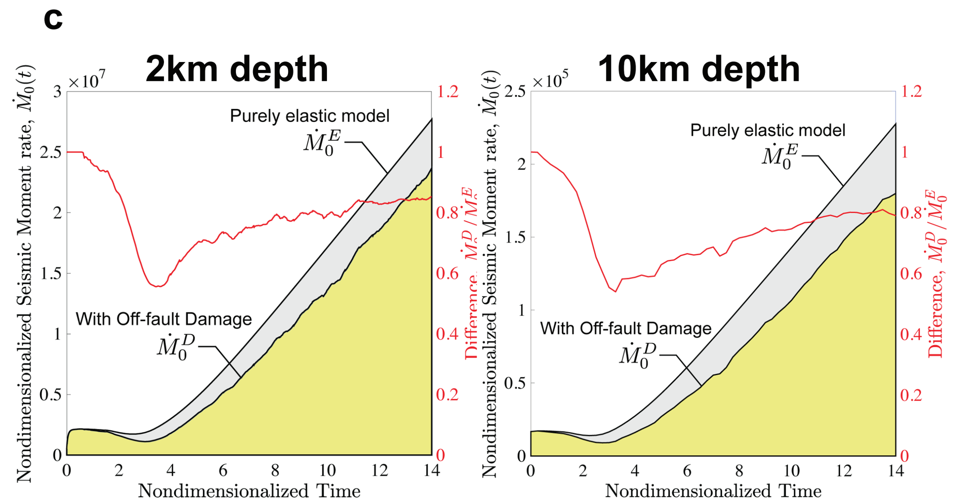

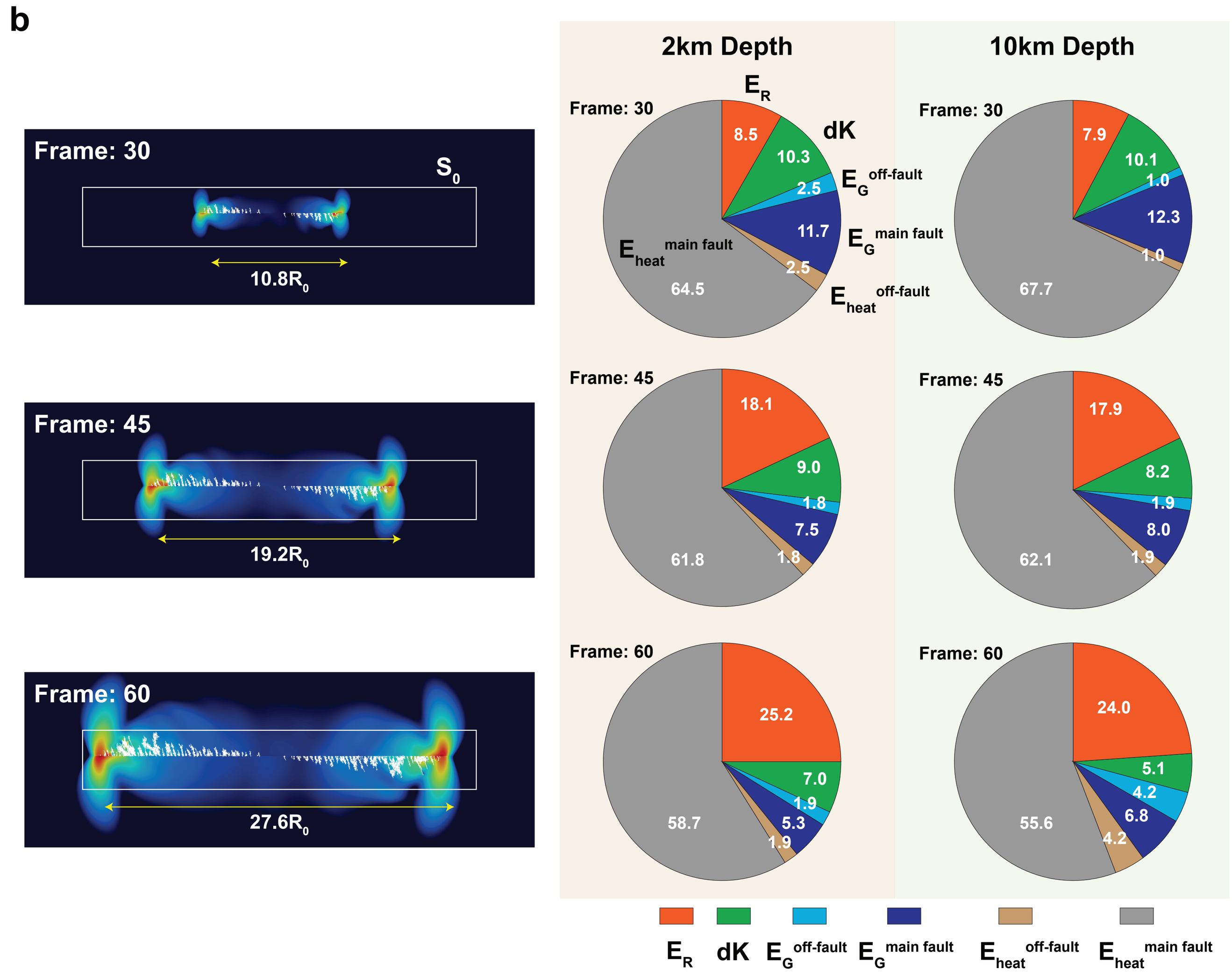

We investigate the balance of overall energy budget associated with the dynamic earthquake rupture including coseismic off-fault damage. (a) The schematic of spatiotemporal overall energy budget. (b) The contributions of energy components accociated with the rupture length. The contributions of energy components are fairly independent of depth. (c) The comparison of Moment-rate function (source time function, STF) with and without off-fault damage. Rate of seismic moment released from the main fault decreases by 20 % due to the decrease of both rupture velocity and slip velocity. **This ratio is independent of depth**.

Damage zone width in depth

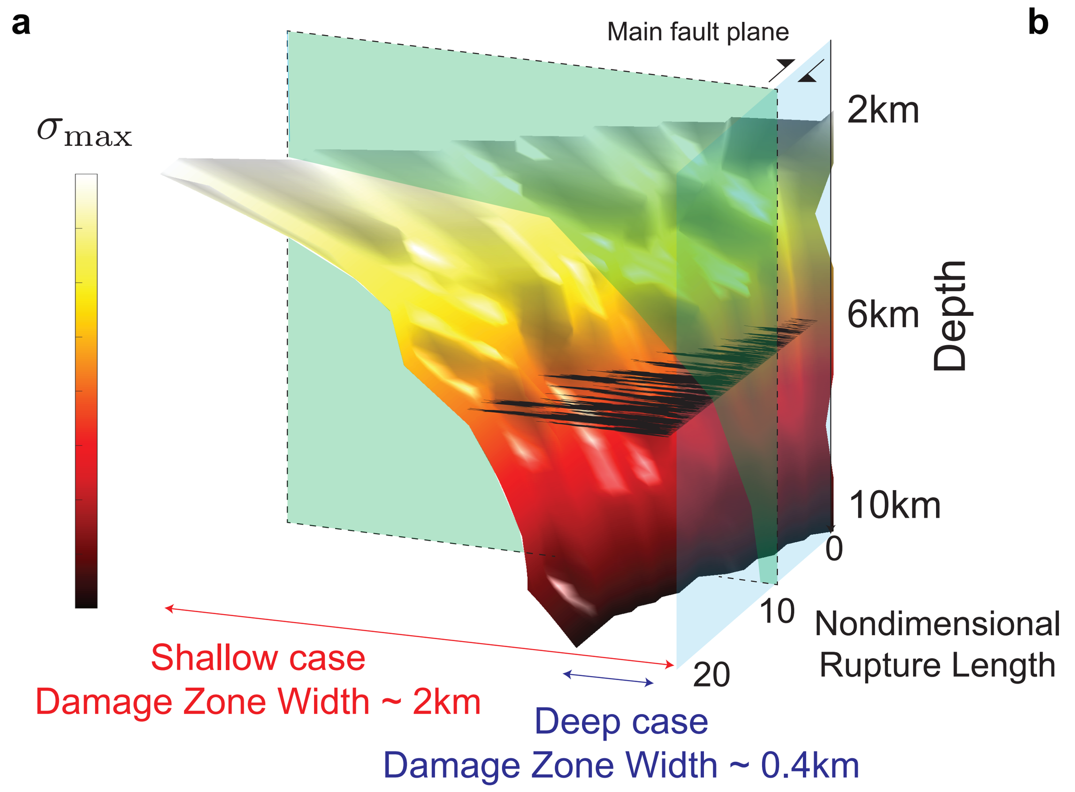

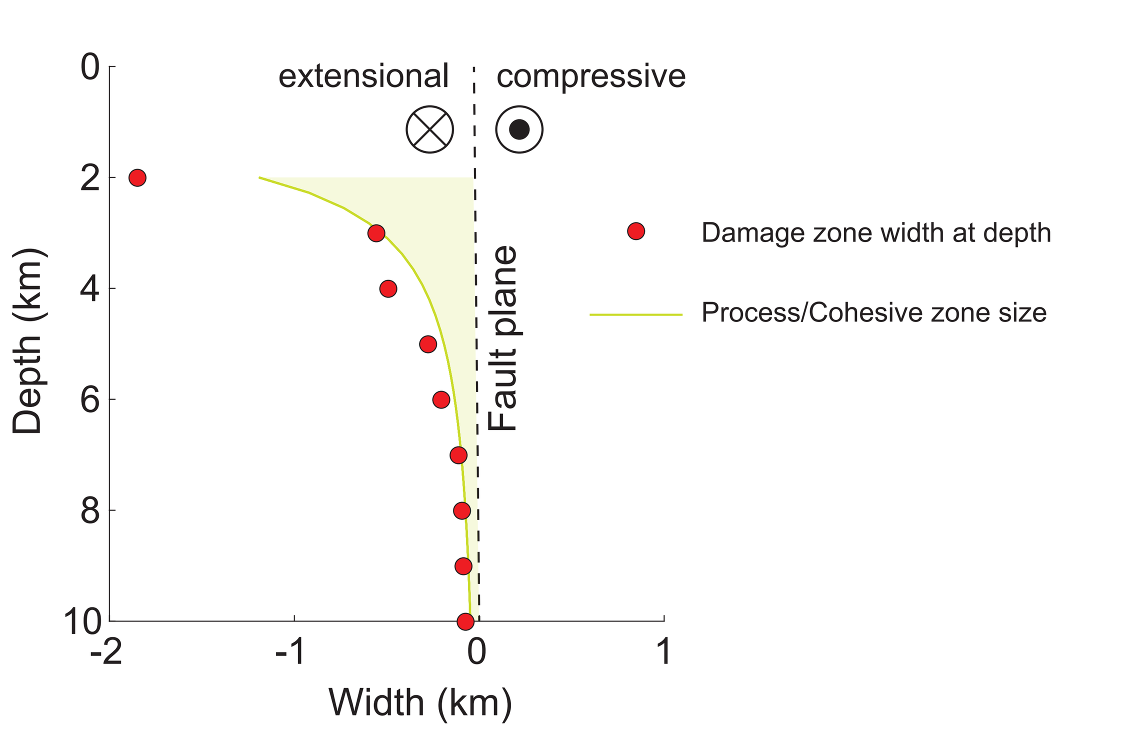

We conducted case study in depth by keeping the fracture energy G_{IIC} on the main fault constant in depth, which leads to smaller process/cohesive zone size in depth. The damage zone width induced by dynamic rupture is generally proportional to the process/cohesive zone size. Thus it sould be narrower in depth. (a) Damage zone width inferred from the 2D case study in depth. We conducted 2D simulations with the pre-stress conditions from 2 km to 10 km depth. We then derive the averaged damage zone width where the secondary off-fault cracks can be generated by dynamic rupture. It shows narrower damage zone in depth, the so called flower like structure. (b) cross-section of the damage zone width in depth. The location is shown in Fig. (a). The damage zone width roughly follows the process zone size estimated with the pre-stress condition associated with depth.

Conclusion

- Our systematic simulations show the implications of dynamically generated secondary crack network on the rupture process, radiated wave field and overall energy budget.
- High-frequency radiation is enhanced by the off-fault crack network, especially in damage zone.
- Dissipated energy on the main fault is dominant compared to the energy dissipated by the off-fault cracks.
- Seismic moment rate decreases due to the secondary crack network and this decrease is significant even when there is a narrow damage zone at depth.
- **Damage zone becomes narrower with depth. However, the effect of off-fault crack network is non-negligible even in the deeper part.**

Acknowledgment

We used the FDEM based software tool, Hybrid Optimization Software Suite – educational version (HOSSedu) developed by Los Alamos National Laboratory.

Z. L. Earl E. Knight, Esteban Rougier, Hybrid optimization software suite (HOSS) – educational version, Tech. Rep. LA-UR-15-27013, Los Alamos National Laboratory (2015).